RSC Advances

PAPER

View Article Online
View Journal | View Issue

Cite this: *RSC Adv.*, 2024, **14**, 15106

Mechanism insight into the high-efficiency catalytic killing of *E. coli* by metal–phenolic network as a nanozyme†

Weiyun Guo, *[abc] Chaoyun Wu,[ab] Guanghui Li,[a] Yonghui Wang,[a] Shenghua He,[a] Jihong Huang,[ac] Xueli Gao[a] and Xiaoyue Yue [b]

Received 18th January 2024
Accepted 28th April 2024

DOI: 10.1039/d4ra00481g

rsc.li/rsc-advances

Glutathione (GSH) as an antioxidant greatly attenuates the reactive oxygen species (ROS) treatment strategy based on peroxidase-activity nanozymes. Therefore, nanozymes with multiple properties that generate ROS and further GSH-depletion functions would be of great benefit to improve antimicrobial efficacy. Herein, focusing on the green, safe and abundant functional prospects of metal–phenolic networks (MPNs) and the strong prospect of biomedical applications, we have synthesized copper tannic acid (CuTA) nanozymes with dual functional properties similar to peroxidase-like activity and GSH depletion. CuTA can catalyze the decomposition of H_2O_2 to hydroxyl radicals (˙OH). In addition, CuTA nanozymes can efficiently deplete available GSH, thus enhancing ROS-mediated antimicrobial therapy. The antibacterial results show that CuTA has an excellent antibacterial effect against *E. coli*.

Introduction

Bacterial infections remain one of the leading causes of death worldwide, posing a substantial threat to human health.[1] *Escherichia coli* (*E. coli*), as a representative of Gram-negative bacteria, is often studied as a bacterial model. Significant progress has been made in recent decades in the prevention of bacterial infections from chemotherapy antimicrobial therapy to nanomedicine. Nanotechnology has achieved considerable success in antimicrobial applications,[2] nanomaterials with biocatalytic activity (known as nanozymes) have undergone extensively significant research and have proven to be stable and biocompatible for use in antimicrobial treatments.[3–5] Nanozymes with efficient peroxidase (POD)-like activity could catalyze hydrogen peroxide (H_2O_2) into more aggressive reactive oxygen species (ROS) for bacterial activation, causing oxidative damage to cellular DNA, proteins, and lipids, leading to cell death.[6] However, to counterbalance the buildup of excess ROS, bacteria cells overexpressed glutathione (GSH) to maintain redox homeostasis that scavenged free radicals, reduced ROS-induced antibacterial activity, and prevented cell death.[7] Therefore, the development of POD-like nanozymes with GSH-depleting functions could be of great benefit in enhancing the antibacterial effect.

Polyphenols have a remarkable contribution in protecting the health of the organism and antioxidants and are linked to numerous biological processes, including as chemical defense, structural support, metal sequestration, pigmentation, and protection against radiation damage.[8] Excellent raw materials for biomedical multifunctional inorganic–organic hybrid materials prepared based on polyphenols are considered potential candidates in energy, environmental, materials, health care and medical fields. In particular, the self-assembled coordination of phenolic ligands with functional metal species to form metal–phenolic networks (MPNs) in emerging supramolecular structures,[9,10] playing a crucial role in biomedical functions.[11] For example, the galloyl and catechol groups in phenols function as pH-responsive multivalent chelating sites and could be coordinated with various metals such as FeIII to achieve protective delivery to probiotics thereby improving human gut health.[12] MPNs are environmentally friendly to green phenolic ligands,[13] and have been addicted in the fields of biointerfaces, particle engineering, adjustable targeted delivery systems, and anticancer antimicrobial therapy.

It is well known that tannic acid (TA) possesses antibacterial, antioxidant, anticarcinogenic and antimutagenic activities. TA is certified as a safe food additive by the US Food and Drug Administration (FDA) and is of particular importance as a natural phenolic ligand (Fig. S1†).[14] The adjacent hydroxyl groups in TA provide chelate sites that may react with different metal ions, and TA has a lot of gallate groups which contributes to ligand-driven cross-linking, resulting in three-dimensionally

[a]*Food and Pharmacy College, Xuchang University, Xuchang 461000, China. E-mail: gwy2002@126.com*

[b]*College of Food and Bioengineering, Zhengzhou University of Light Industry, Zhengzhou 450001, China*

[c]*Food Laboratory of Zhongyuan, Luohe 462000, China*

† Electronic supplementary information (ESI) available: SEM and TEM images of CuTA nanozyme, pH and temperature optimization of the catalytic activity of CuTA peroxidases, growth curve analysis of *E. coli* with or without the presence of various CuTA concentrations, the images showing MIC measurement results. See DOI: https://doi.org/10.1039/d4ra00481g

stable MPNs. The polydentate ligand of TA tends to mix with the Cu^{2+} through a fast coordination rate to yield linked metal–polyphenol complex such as CuO–TA as the TA contributes more oxygen to the structures. The fast coordination causes the aggregation of the nanostructures. By taking into account the antibacterial activity of TA, it might be feasible and highly interesting to integrate bactericidal features into TA-stabilized MPNs. The definite antibacterial function and biosafety of copper make it an excellent metal ion candidate for the construction of coordination polymers.[15] Herein, based on a self-assembly strategy we synthesized copper tannic acid (CuTA) nanozymes, although CuTA has been used in antibacterial research,[16] its enzymatic catalytic properties have not been resolved. Not only CuTA nanozymes could destroy the cell wall through direct contact, allowing easier leakage of intracellular material, but also catalyze the production of $^{\bullet}OH$ from endogenous H_2O_2 and induce GSH depletion to achieve more effectiveness of eradication of *E. coli*. As TA is just one of several natural polyphenols, the MPNs approach could provide a new green pathway to produce sophisticated functional materials, bridging the gap between biology and nanotechnology.

Results and discussion

Structure characterizations and morphology of CuTA nanozymes

CuTA nanozymes were created through oxidative interaction of copper ions and TA self-assembly and were based on a strong chelating ability to form MPNs. The self-oxidation of TA was considerably enhanced in the presence of Cu^{2+}.[18,19] During coordination with Cu^{2+}, both the highly reactive semi-quinones and quinones formed by oxidation of catechol moiety of TA undergo self-polymerization. The evolution of the CuTA morphology is mainly a consequence of the pH of the reaction and the Cu^{2+} concentration. Larger reaction pH encourages deprotonation of the catechol group, while higher Cu^{2+} concentrations allow the development of CuTA coordination networks.[17] Cu^{+} ions enabled an efficient POD-like reaction, but obtaining stable Cu^{+} ions is demanding. Fortunately, the coordination of Cu^{2+} ions with polyphenols was a workable strategy to produce Cu^{+} ions.[20] The defined flower-shaped nanosheets of CuTA were validated by morphology observations utilizing SEM and TEM (Fig. 1a, b, S2 and S3†). SEM imaging showed that CuTA consists of mostly needle-like lamellae assembled with a width of about 200 nm and aggregated to form flower-like structures. The morphology could effectively penetrate the thin cell wall of *E. coli* when physically interacting with them. The CuTA nanozymes' XRD pattern shown in Fig. 1c revealed a distinctive crystalline structure that distinguished it from other Cu-based materials (such as Cu, Cu_2O, CuO and $Cu(OH)_2$). The results of FTIR and XPS further verified the coordination between Cu^{2+} and TA. The generated CuTA nanozymes displayed splitting and shifting of absorption in the FTIR spectrum as compared to TA itself because of the oxidation of TA and subsequent coordination to Cu^{2+}. The HO–C vibration of TA was disrupted by the coordination of the phenolic moiety to Cu^{2+}, displaying an absorption shift in the fingerprint region and absorption splitting with a center point at 3394 cm^{-1}. The infrared activation vibration mode of Cu(II)–O was shown by three distinct absorption peaks at 601, 479, and 420 cm^{-1}.[21,22] Under the influence of metal bonding, the curves of 300 to 650 cm^{-1} were flat compared to the abrupt peaks of pure TA (Fig. 1d).[16] Further, the results of XPS were used to determine the concentration and oxidation state of Cu. The Cu, C, and O atomic ratios in the CuTA nanozymes were 20.99%, 20.67%, and 53.28% (Fig. 1e). The major Cu $2p_{3/2}$ and Cu $2p_{1/2}$ peaks were seen in the fine spectrum of Cu 2p (Fig. 1f), along with shake-up satellite peaks at 942.4 and 962.5 eV, respectively. They demonstrated that 17.14% of Cu was still in +2 state while 68.52% was in +1 state. As shown in Fig. S4,† thermogravimetric analysis (TGA) curves of CuTA are with two degradative weight losses approximately at 100 and 200 °C, respectively. At the pyrolysis temperature increases to 400–700 °C, the carbonisation of CuTA is considered to be basically completed. Furthermore, the unique mixed-valence state facilitated POD-like action in a moderately acidic environment (Fig. S5†).

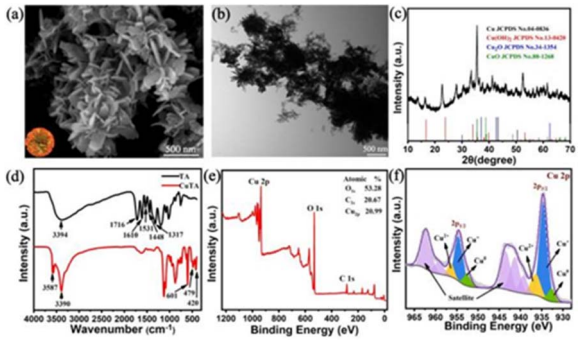

Fig. 1 Synthesis and compositional characterizations of CuTA. (a) SEM image. (b) TEM image. (c) XRD pattern. (d) FTIR spectra. (e) XPS spectrum. (f) High-resolution spectra of Cu 2p.

The POD-like activity and GSH depletion of CuTA

According to previous reports, the endogenous H_2O_2 in *E. coli* cells could be accelerated into highly harmful free radicals by nanozymes,[16,23] *E. coli* continually produces 10 to 15 μM s^{-1} of endogenous H_2O_2 when it develops on typical substrates due to the unintentional autoxidation of redox enzymes.[24] Meanwhile, endogenous H_2O_2 could be attached to the surface of microbial cell walls or free in the system, providing a potential catalytic substrate for CuTA, which was a key step leading to cell death. Therefore, it was certainly significant to verify whether CuTA has excellent POD-like activity. To make sure that CuTA nanozymes with a high Cu^{+} content could function as POD-like agents to induce the decomposition oh H_2O_2 to produce $^{\bullet}OH$, thereby catalyzing the production of blue color or absorption at 652 nm from TMB (Fig. 2a). As indicated in Fig. 2b, the absorbance of only CuTA + TMB and H_2O_2 + TMB was negligible, indicating that no oxidation reaction occurred. The color of the mixture changed significantly with the addition of CuTA + H_2O_2, and the characteristic absorption peak at 652 nm was caused by oxTMB. Probing with different concentrations of

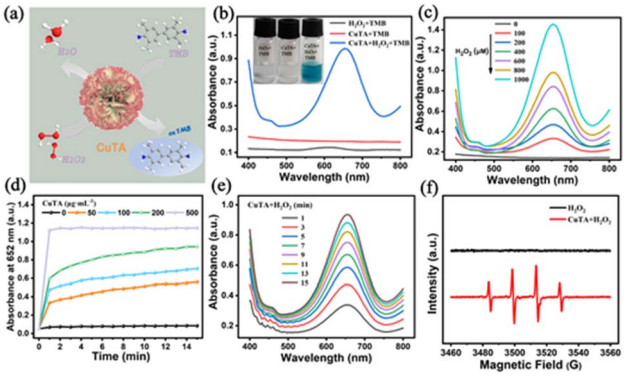

Fig. 2 *In vitro* performance of POD-like activity of CuTA nanozymes. (a) Schematic illustration for CuTA-mediated ˙OH generation. (b) UV-vis absorption spectra of the catalyzed oxTMB with different treatments. The illustration is a photograph of the corresponding solution. (c) UV-vis absorption spectra changes of oxTMB under different H_2O_2 concentrations. (d) Time-dependent absorbance changes with different CuTA concentration at 652 nm as a result of the catalyzed oxidation of TMB at room temperature (25 °C). (e) UV-vis absorption spectra of the catalyzed oxTMB under different time. (f) ESR spectra of H_2O_2 and CuTA + H_2O_2.

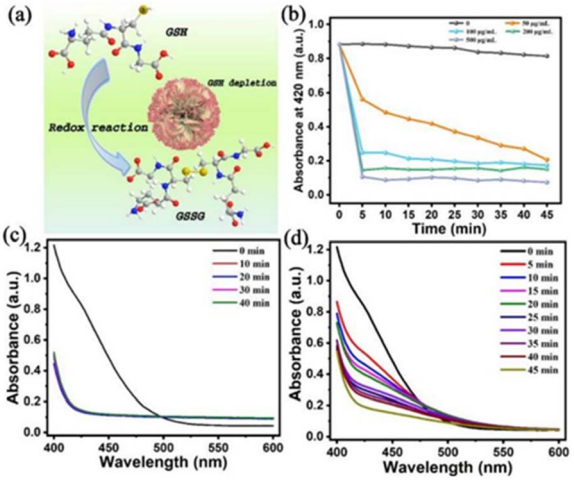

Fig. 3 *In vitro* performance of GSH depletion of CuTA nanozymes. (a) Schematic illustration for GSH consumed by CuTA. (b) UV-vis absorption spectra of GSH depleting abilities of different CuTA concentrations with DTNB as the trapping agent of –SH in GSH. UV-vis absorption spectra of GSH depleting abilities of (c) CuTA (500 μg mL^{-1}) and (d) CuTA (50 μg mL^{-1}) in different time with DTNB as the trapping agent of –SH in GSH.

H_2O_2 as catalytic substrate, the results showed that the generated ˙OH steadily increased as the concentration of H_2O_2 rose, and the absorbance at 652 nm increased significantly, showing the dependence on H_2O_2 concentration (Fig. 2c), indicating that CuTA could effectively catalyze the decomposition of H_2O_2 to produce ˙OH. The POD-like catalytic performance of CuTA was influenced by concentration, reaction time, much like that of other POD mimics. As shown in Fig. 2d, different concentrations of CuTA produced different catalytic effects and showed a concentration dependence, with higher CuTA concentrations providing stronger catalytic effects. The oxidation effect and absorbance values presented were more pronounced with increasing time (Fig. 2e). Large amounts of ˙OH were generated by CuTA nanozymes, which had been demonstrated apart from the colorimetric methods. ESR with the spin traps DMPO was also applied to directly capture ˙OH, the characteristic ˙OH (1 : 2 : 2 : 1) signals may be readily observed in the CuTA–H_2O_2 solution (Fig. 2d), which further proved that CuTA acts as an excellent POD-like catalyst for the generation of ˙OH. As one of the most potent free radicals capable of oxidation, ˙OH might interact with practically all biological components.[25] Free radicals could cause oxidative damage by trapping hydrogen in proteins to form unsaturated fatty acids, or by performing lipid peroxidation reactions.[26]

Another characteristic was the existence of GSH in the form of intracellular free thiols, which served to shield bacterial cells from oxidative damage brought on by free radicals.[7] According to scientific reports, the physiological concentration of GSH in *E. coli* cytoplasm ranges from 3.5 mM to 6.6 mM.[27] Therefore, if GSH is not quickly depleted, the antimicrobial effectiveness of ROS-based treatments will be seriously jeopardized. Therefore, it is important to deplete GSH in order to simultaneously improve the efficacy of ROS-based therapy. Copper-based catalysts had good GSH depletion capability, enhancing the antimicrobial impact of ROS-related treatments.[28] We wondered if the produced CuTA nanozymes might be available for GSH depletion. Excess GSH was incubated with various quantities of CuTA nanozymes, and the residual GSH was detected at various times by DTNB ((–SH) indicator) (Fig. 3a).[29] The results showed that the higher CuTA concentration, the faster decrease in characteristic absorbance at 420 nm, the less –SH in the residual GSH and the more GSH was oxidized to GSSG (Fig. 3b). After 10 min of reaction with CuTA (500 μg mL^{-1}), no longer visible was the distinctive peak of DTNB (Fig. 3c). GSH was entirely consumed within 45 min even when the CuTA concentration was as low as 50 μg mL^{-1} (Fig. 3d), showing the concentration-dependent manner of CuTA. GSH could still be completely consumed even when CuTA content was substantially lower than GSH content. It might be due to the fact that CuTA act as a GSH oxidase (GSH-OXD)-like mimetic enzyme, which may effectively deplete GSH at a lower concentration, producing an acceptable GSH-depletion capability. The equation was supposed to how GSH was being depleted,

$$2Cu^{2+} + 2GSH = 2Cu^{+} + GSSG + 2H^{+} \quad (1)$$

GSH depletion decreases ROS annihilation to enhance ROS-mediated effects by disrupting cellular antioxidant defense systems.[30]

Antibacterial activity evaluation

In vitro antibacterial performance of CuTA was studied using *E. coli* as a target. The MIC of CuTA against *E. coli* was 0.8 mg mL^{-1} (Fig. S6 and S7†). The control cells showed a typical growth pattern, whereas *E. coli* treated with CuTA showed a decreased

growth rate and took longer to reach the stabilization phase in a concentration-dependent manner. Considering the above-mentioned excellent features of CuTA, the possibility of using CuTA as a potential nano-antibacterial agent in combination with the POD-like catalytic and GSH-depletion effect to synergistically ablating bacteria was then investigated. The antibacterial activity of CuTA was assessed by a standard plate count method. The photographs in Fig. 4a showed the quantification of bacterial colonies of *E. coli* treated with different concentrations of CuTA alone and the corresponding bacterial viability. It was discovered that CuTA possessed some degree of killing power against *E. coli*, and the antibacterial power varied with CuTA concentration. When bacteria were treated with the CuTA nanozymes at the 100 μg mL^{-1} concentration of CuTA within 15 min, the killing rate achieved nearly 50%, with an elimination rate of 79.85% for CuTA powder at a concentration of 200 μg mL^{-1} and nearly 99.99% for 500 μg mL^{-1} (Fig. 4b). Compared to Cu^{2+} or TA alone (Fig. S8†), the antibacterial effect of CuTA was more obvious at the same component contents. And the comparisons with the past related examples were shown in Table S1.† The needle-like flower-like structure of CuTA provided an effective weapon for its antibacterial effect to puncture the cell wall of *E. coli* from the lethal effect of ˙OH high expression caused by the POD-like reaction of endogenous H_2O_2 and multivalent Cu ions in *E. coli*.

In order to decipher the antibacterial pathways of CuTA, morphological changes of bacteria closely connected to bacterial death were further visualized. It was conspicuous that the control *E. coli* cells displayed rod-like shapes with smooth surfaces and intact membrane structure (Fig. 4c), whereas CuTA treatment caused different degrees of surface deformation in the *E. coli* cells, including wrinkles and fissures, and even excessive efflux of cellular contents (Fig. 4d), implying that CuTA nanozymes prompted the breakdown of *E. coli* cell membranes and additional cytoplasm leaking. Furthermore, to verify the role of GSH in maintaining ROS homeostasis and protecting cells from oxidative damage by ROS, the antibacterial efficacy was significantly weakened to a certain extent by the addition of excess GSH to the system of CuTA killing *E. coli* (Fig. 4e), indicating that GSH had the ability to scavenge ROS. As a result, the GSH-depleting function of CuTA further increased the antibacterial effectiveness by decreasing the ROS scavenging capacity of GSH and its ability to protect bacteria. On this basis, the possible combined antibacterial mechanisms of CuTA were proposed: (1) the destructive physical contraction of bacteria with rough edges of CuTA increased due to the component movement; (2) CuTA could act as a POD-like nanozyme that efficiently produced ˙OH in presence of H_2O_2, causing cell oxidative damage; (3) CuTA could also act as GSH-OXD-like nanozymes depleted GSH in the internal environment of *E. coli*, enhancing the efficacy of antimicrobial therapy. Therefore, the antimicrobial mechanisms of CuTA primarily consisted of destructive physical interaction, ROS generation, and GSH depletion (Fig. 4f).

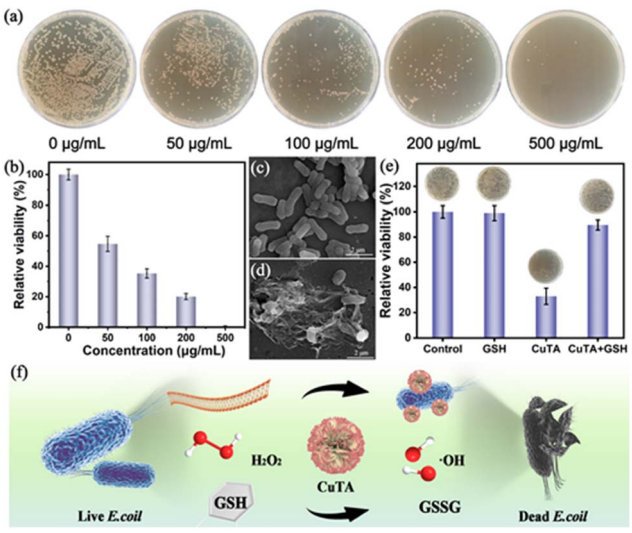

Fig. 4 Evaluation of the antibacterial effect of CuTA. (a) Photographs of *E. coli* colonies after treatment with different concentrations of CuTA. (b) Quantitative antibacterial evaluation of different CuTA concentrations. (c) SEM images of the control bacteria of *E. coli* and (d) treated *E. coli*. (e) Quantitative and plate results for different treatments of *E. coli*. (f) Schematic diagram of the mechanism of killing *E. coli*.

Conclusions

In conclusion, dual POD-like and GSH-depletion of CuTA nanozymes synthesized through the self-assembling of copper–tannic acid-coordinated strategy were used for killing *E. coli*. CuTA interacted with bacterial cells, destroyed the membranes, and catalyzed endogenous H_2O_2 to generate ˙OH, causing oxidative damage to cells. More importantly, CuTA depleted GSH, thereby disrupting the intercellular protection system of *E. coli* and predisposing them to death. This work was an antibacterial strategy based on the synergistic effect of catalytic reaction and GSH depletion, providing a feasible multi-properties antibacterial treatments.

Experimental

Materials

Cupric sulfate anhydrous ($CuSO_4$), 3,3′,5,5′-tetramethylbenzidine (TMB), GSH (reduced), 5,5-dimethyl-1-pyrroline *N*-oxide (DMPO) were purchased from Aladdin Chemical Reagent Co., Ltd. Tannic acid (TA) and 5,5′-dithiobis(2-nitrobenzoic acid) (DTNB) were purchased from Sigma-Aldrich Co., Ltd. Sodium Hydroxide (NaOH) were purchased from Guangdong Guanghua Sci-Tech Co. Ltd. Phosphate buffer saline (PBS) purchased from Shanghai yuan ye Bio-Technology Co., Ltd. Without additional purification, all chemical reagents were employed in their original form. Deionized water (18.2 M cm, Millipore) was used to make all of the aqueous solutions that were employed in the experiments.

Synthesis of CuTA nanozyme

A method of oxidative coupling assembly was used to create CuTA nanozymes.[17] In a typical synthesis, a homogenous

solution was created by dissolving 54 mg of TA and 1.750 g of $CuSO_4$ in 100 mL of deionized water. The solution was heated to 60 °C and maintained for 3 hours after having its pH adjusted to 7.4 by 2 M NaOH. Centrifugation (8000 rpm, 10 min) was used to separate the product, and washed with deionized water three times to remove impurities. Finally, the purified light green product was freeze-dried under vacuum for characterization and further experiments.

Apparatus and characterization

The UV-visible absorption spectra was collected by UV-2550 UV-vis spectrophotometer (Shimadzu, Japan). An S-4800 (Hitachi, Japan) was used to carry the field emission scanning electron microscopy (SEM) images. A transmission electron microscope (TEM) (JEM 1230, Japan) was used to take pictures of the materials. Using a Cu Kα (1.5418 Å) source produced powder X-ray diffraction (XRD) patterns (Bruker D8 Advanced Diffractometer System, Germany). X-ray photoelectron spectroscopy (XPS) data were recorded on a Thermo Scientific ESCALAB 250 equipped with an Al Kα source (1486.6 eV). Fourier transform infrared (FTIR) spectroscopy was used to examine the functional groups by Bruker Vertex 70 (Germany). Electron spin resonance (ESR) was measured using a JES-FA200 ESR spectrometer (JEOL, Japan). Large Stackable Shaker Incubator (ZDZY-BF8/BS8) was purchased from Shanghai Zhichu Instrument Co., Ltd.

POD-like activity of CuTA nanozyme

The H_2O_2 catalytic oxidation of chromogenic substrates TMB was used to evaluate the POD-like activity of CuTA. Typically, the substrate TMB (20 mM, 20 μL), H_2O_2 (10 mM, 20 μL), 0.1 mg mL^{-1} CuTA (20 μL) were fully mixed in NaAc–HAc buffer (0.02 M) of a 200 μL system. After 15 minutes of reaction at room temperature. UV-vis was used to gauge the reaction system's absorbance at 652 nm. Then, the CuTA enzyme activity curve at various doses was determined. Additionally, the $^{\bullet}OH$ generated by CuTA was detected by ESR spectroscopy and was detected using DMPO as a free radical probe.

GSH depleting with CuTA

The CuTA nanozymes with different concentrations were mixed with GSH (1.0 mM) at room temperature (25 °C). To find the –SH of GSH, 100 μL of the mixture was pipetted at various time intervals, diluted to 900 μL in PBS (pH 7.4), and then added.

Bacterial culture

E. coli (ATCC 25922) was shaken at 220 rpm for 12 hours at 37 °C (ZDZY-BF8/BS8) before being further diluted in PBS (0.01 M) to 1×10^7 CFU mL^{-1}. The optical density value at a wavelength of 600 nm (OD_{600} nm) was used to assess the bacterial concentration (OD_{600} nm $\sim$ 0.50).

Determination of minimum inhibitory concentration (MIC)

Using the broth dilution technique in accordance with the recommendations of the Clinical and Laboratory Standards Institute guidelines (CLSI M7-A9), the MICs of CuTA against *E. coli* (ATCC 25922) were calculated. In a nutshell, 200 μL of a diluted bacterial strain culture with a final cell concentration of around 5×10^5 CFU mL^{-1} was put into each well of a 96-well plate. To achieve final concentrations of 0.8, 0.4, 0.2, 0.1, 0.05, or 0 mg mL^{-1}, CuTA solution was then added to each well. Following a 24 hour incubation period at 37 °C for the samples, the optical density at 600 nm (OD_{600} nm) was calculated using a microplate reader.

In vitro antibacterial activity of CuTA

To explore the relationship between the dosage of CuTA and the sterilizing rate towards *E. coli*, the concentration of CuTA was set at 0, 50, 100, 200, and 500 μg mL^{-1}. The bacteria suspension (450 μL, 1×10^7 CFU mL^{-1}) was mixed with CuTA in 2.0 mL centrifuge tubes. The CuTA-free LB plates were used as the control group. The samples were diluted with PBS for photos and counting. The LB agar plates were streaked with 100 L of bacteria dilution from each group and incubated at 37 °C for 18 hours (colony size suitable for observation or counting). Triplicates of each test were run.

Characterization of bacterial cells

Following the aforementioned antibacterial test, *E. coli* was centrifuged three times at 3000 rpm for five minutes with PBS to remove any remains, and it was then fixed with 1 mL of glutaric dialdehyde-fixed liquid for six hours at 4 °C in the dark. After that, a graduated series of ethanol (30, 50, 70, 80, 90, and 100%) was used to dehydrate the bacterial cells for 10 min. Then replaced once with isoamyl acetate (10 min) and stored in it. The specimen was fixed and dehydrated as described above, then examined using the SEM apparatus.

Conflicts of interest

The authors declare that the research was conducted in the absence of any commercial or financial relationships that could be construed as a potential conflict of interest.

Acknowledgements

We acknowledge the funding support from the Major Science and Technology Projects in Henan Province, China (ID No. 201300110300), Key Scientific Research Projects of Universities in Henan Province (ID No. 22B550017), the Science and Technology Development Project of Henan Province (232102111061 and 222102310355) and the training program for Young Backbone Teachers in Colleges and Universities in Henan Province, China (ID No. 2019GGJS216).

References

1 H. Koo, R. N. Allan, R. P. Howlin, P. Stoodley and L. Hall-Stoodley, *Nat. Rev. Microbiol.*, 2017, **15**, 740–755.
2 Y. Wang, Y. Yang, Y. Shi, H. Song and C. Yu, *Adv. Mater.*, 2020, **32**, 1904106.

3 Y. Zhang, F. Wang, C. Liu, Z. Wang, L. Kang, Y. Huang, K. Dong, J. Ren and X. Qu, *ACS Nano*, 2018, **12**, 651–661.
4 S. Dong, Y. Dong, T. Jia, S. Liu, J. Liu, D. Yang, F. He, S. Gai, P. Yang and J. Lin, *Adv. Mater.*, 2020, **32**, 2002439.
5 F. Wu, Y. Du, J. Yang, B. Shao, Z. Mi, Y. Yao, Y. Cui, F. He, Y. Zhang and P. Yang, *ACS Nano*, 2022, **16**, 3647–3663.
6 J. Xi, G. Wei, L. An, Z. Xu, Z. Xu, L. Fan and L. Gao, *Nano Lett.*, 2019, **19**, 7645–7654.
7 A. Bansal and M. C. Simon, *J. Cell Biol.*, 2018, **217**, 2291–2298.
8 S. Quideau, D. Deffieux, C. Douat-Casassus and L. Pouységu, *Angew. Chem., Int. Ed.*, 2011, **50**, 586–621.
9 M. J. Mitchell, M. M. Billingsley, R. M. Haley, M. E. Wechsler, N. A. Peppas and R. Langer, *Nat. Rev. Drug Discovery*, 2021, **20**, 101–124.
10 Z. Zhang, L. Xie, Y. Ju and Y. Dai, *Small*, 2021, **17**, 2100314.
11 W. Sang, Z. Zhang, G. Wang, L. Xie, J. Li, W. Li, H. Tian and Y. Dai, *Adv. Funct. Mater.*, 2022, 2113168.
12 G. Fan, P. Wasuwanich, M. R. Rodriguez-Otero and A. L. Furst, *J. Am. Chem. Soc.*, 2022, **144**, 2438–2443.
13 H. Ejima, J. Richardson Joseph, K. Liang, P. Best James, P. van Koeverden Martin, K. Such Georgina, J. Cui and F. Caruso, *Science*, 2013, **341**, 154–157.
14 S. Shi, W. Zhang, X. Ren, M. Li, J. Sun, G. Li, Y. Wang, T. Yue and J. Wang, *Carbohydr. Polym.*, 2019, **226**, 115283.
15 X. Zhang, Z. Zhang, Q. Shu, C. Xu, Q. Zheng, Z. Guo, C. Wang, Z. Hao, X. Liu, G. Wang, W. Yan, H. Chen and C. Lu, *Adv. Funct. Mater.*, 2021, **31**, 2008720.
16 J. Li, J. Li, J. Wei, X. Zhu, S. Qiu and H. Zhao, *ACS Appl. Mater. Interfaces*, 2021, **13**, 10446–10456.
17 S. Lin, Y. Cheng, H. Zhang, X. Wang, Y. Zhang, Y. Zhang, L. Miao, X. Zhao and H. Wei, *Small*, 2020, **16**, 1902123.
18 Z. Chen, C. Wang, J. Chen and X. Li, *J. Am. Chem. Soc.*, 2013, **135**, 4179–4182.
19 M. Mochizuki, S.-i. Yamazaki, K. Kano and T. Ikeda, *Biochim. Biophys. Acta, Gen. Subj.*, 2002, **1569**, 35–44.
20 Y. Wang, Y. Ding, D. Yao, H. Dong, C. Ji, J. Wu, Y. Hu and A. Yuan, *Small*, 2021, **17**, 2006231.
21 G. Zou, H. Li, D. Zhang, K. Xiong, C. Dong and Y. Qian, *J. Phys. Chem. B*, 2006, **110**, 1632–1637.
22 D. Chen, G. Shen, K. Tang and Y. Qian, *J. Cryst. Growth*, 2003, **254**, 225–228.
23 S. Korshunov and J. A. Imlay, *Mol. Microbiol.*, 2010, **75**, 1389–1401.
24 S. Ravindra Kumar and A. Imlay James, *J. Bacteriol.*, 2013, **195**, 4569–4579.
25 G. Lyngsie, L. Krumina, A. Tunlid and P. Persson, *Sci. Rep.*, 2018, **8**, 10834.
26 L.-J. Su, J.-H. Zhang, H. Gomez, R. Murugan, X. Hong, D. Xu, F. Jiang and Z.-Y. Peng, *Oxid. Med. Cell. Longevity*, 2019, **2019**, 5080843.
27 P. Koprowski and A. Kubalski, *Pfluegers Arch.*, 1999, **438**, 361–364.
28 Y. Liu, J. Wu, Y. Jin, W. Zhen, Y. Wang, J. Liu, L. Jin, S. Zhang, Y. Zhao, S. Song, Y. Yang and H. Zhang, *Adv. Funct. Mater.*, 2019, **29**, 1904678.
29 L. Feng, B. Liu, R. Xie, D. Wang, C. Qian, W. Zhou, J. Liu, D. Jana, P. Yang and Y. Zhao, *Adv. Funct. Mater.*, 2021, **31**, 2006216.
30 Y. Cheng, C. Wen, Y.-Q. Sun, H. Yu and X.-B. Yin, *Adv. Funct. Mater.*, 2021, **31**, 2104378.